RSC Advances

ROYAL SOCIETY OF CHEMISTRY

www.rsc.org/advances

Comparisons between gelatin-tussah silk fibroin/hydroxyapatite and gelatin-*Bombyx mori* silk fibroin/hydroxyapatite nano-composites for bone tissue engineering

Jiabing Ran, Jingxiao Hu, Guanglin Sun, Si Chen, Li Chen, Xinyu Shen*, Hua Tong*

Key Laboratory of Analytical Chemistry for Biology and Medicine, Ministry of Education, College of Chemistry and Molecular Sciences, Wuhan University, Wuhan, 430072, China

*Corresponding author: Hua Tong (E-mail address: sem@whu.edu.cn; Tel: +86 027 68764510; Fax: +86 027 68752136)

*Corresponding author: Xinyu Shen (E-mail address: shenxy@whu.edu.cn; Tel: +86 027 68764510; Fax: +86 027 68752136)

Abstract:

In this research, gelatin-tussah silk fibroin/hydroxyapatite (GEL-TSF/HAp), gelatin-*Bombyx mori* silk fibroin/hydroxyapatite (GEL-BMSF/HAp), and gelatin/hydroxyapatite (GEL/HAp) nano-composites were synthesized by a novel *in situ* precipitation method. Characterizations, including surface morphology, elemental composition and distribution, structure of crystalline phase, mechanical strength, thermal stability, and *in vitro* cytocompatibility, were carried out. Investigations on the crystalline phase showed that rod-like HAp crystallites in GEL-TSF/HAp composite had higher aspect ratio than those in GEL-BMSF/HAp composite and GEL/HAp composite. In addition, GEL-TSF/HAp composite also presented better thermal stability than the other two composites revealed by differential thermal analysis (DTA) and thermogravimetric analysis (TGA). Mechanical properties testing indicated that GEL-TSF/HAp composite had higher elastic modulus at low strain and higher compressive modulus at high strain simultaneously than the other two composites. *In vitro* cell culture showed that MG63 osteoblast-like cells on GEL-TSF/HAp membrane took on higher proliferative potential than those on GEL-BMSF/HAp membrane. These results indicated that compared to GEL-BMSF/HAp composite, GEL-TSF/HAp composite was more suitable for bone tissue engineering (BTE) applications.

Keywords: Tussah silk fibroin; *Bombyx mori* silk fibroin; Mechanical strength; Bone tissue engineering

1. Introduction

Currently, tumor resection, trauma, and selective surgery have posed great challenges to the repair of critical-sized bone defects.[1] Conventional bone tissue replacements (*e.g.,* autografts, allografts) have encountered a lot of problems (limited availability of bone grafts, donor site morbidity, risk of infection, *etc.*). Therefore, they cannot meet high performance demands necessary for today's patient.[2] BTE utilizes bone substitutes, which combine cells, scaffolds, and bioactive factors together, to induce *in situ* new bone formation *in vivo* and has proven to be a promising alternative route.[3, 4]

In BTE, biomaterial scaffolds not only act as carriers for cells and bioactive factors but also provide temporary mechanical function, facilitate mass transporting, and aid biological delivery and bone tissue regeneration.[5] Therefore, developing ideal biomaterial scaffolds is of great significance. As a nano-composite, natural bone comprises of a protein-based soft hydrogel template (*i.e.,* collagen, water, and noncollagenous proteins including laminin, fibronectin, vitronectin, *etc.*) and hard inorganic components mainly composed of nano-HAp.[6] And collagen fibers and nano-HAp are tightly integrated in a hierarchical architecture over several length scales.[7] Hence, biomaterial scaffolds, especially the natural biopolymer/nano-HAp composite scaffolds that mimic the structure and composition of bone tissue at nanoscale, have gained much attention in BTE filed. Though collagen/nano-HAp composite should have been an ideal candidate, the low cost efficiency restricted its widespread usage.[8] Accordingly, investigators have been keeping on seeking for new

substitutes for collagen.[9-12] Herein, Riccardo and Puppi summarized the favorable and unfavorable properties of many natural biopolymers (chitosan, silk fibroin, collagen, hyaluronan, gelatin, alginate, starch, bacterial cellulose, and dextran, *etc.*), which could be applied in BTE.[13, 14]

Gelatin (GEL), derived from collagen, has similar composition and structure with collagen. To date, GEL has been widely used in clinics for wound dressings, pharmaceuticals, and adhesives for its bioaffinity, lack of antigenicity, hydrogel characteristics, formability, and cost efficiency.[15] GEL seems to be able to substitute for collagen. However, GEL/HAp nano-composites suffer from poor mechanical strength.[9] In order to make up this defect, silk fibroin (SF), owing excellent viscoelastic properties, was utilized as an organic reinforcement phase.[16]

SFs are generally defined as protein polymers and differ widely in composition, structure, and properties depending on specific source. Different SFs have different amino acid sequences, which correspond to different bioaffinity, and exhibit mechanical properties tailored to their specific functions.[17] In this research, domestic SF (*i.e., Bombyx mori* silk) and wild SF (*i.e.,* tussah silk) were employed. BMSF is a kind of linear polypeptide composed of 17 amino acids, mainly nonpolar ones such as alanine and glycine.[18] In the medical field, BMSF with β-sheet structure has long been used as surgical sutures for its outstanding biocompatibility, water vapor permeability, biodegradability, and minimal inflammatory reaction.[19, 20] Differing from BMSF, TSF is a kind of wild silk, and its amino acid composition includes more alanine (Ala), aspartic acid (Asp), and arginine (Arg) content but less glycine (Gly).[21, 22]

Furthermore, the crystallinity of TSF is higher than that of BMSF, and TSF contains more tripeptide sequence of Arg-Gly-Asp (RGD). The RGD tripeptide sequence could act as a biological recognition signal and was very effective for several biotechnological and biomedical applications (*e.g.,* enzyme immobilization, matrix for mammalian cell culture, wound covering, and artificial skin).[23-25] Most SFs share a composite structure with crystalline and noncrystalline compounds, and the high degree of interlinking between the two fractions leads to the viscoelastic properties of silks.[16] The amino acid sequence of crystalline regions of BMSF and TSF consists of —$(Gly\text{-}X)_n$— (X represents Ala or Trp residues) and —$(Ala)_n$— sequence, respectively. Thus, TSF has a more compact molecular structure and is expected to have better mechanical strength.[26, 27] From previous investigations, researchers also found that pure SF/HAp composites could not meet the requirements of bone substitution for its insufficient formability and flexibility.[28-30] In order to overcome this obstacle, SF and GEL were hybridized to function as a composite organic phase.

The objective of this study was to prepare an ideal bone substitute by combining the superiorities of GEL and SF together. Considering that the molecular composition, molecular structure, and crystallinity of TSF and BMSF were different, and it might influence the crystal size and structure of HAp, which were related to the mechanical strength, thermal stability, and cytocompatibility of composites, investigations on the crystalline phase of composites were carried out especially. In addition, comparisons between GEL-TSF/HAp composite and GEL-BMSF/HAp composite were also made in detail. The structural and compositional characterizations of composites were

performed to analyze the mediation effects of organic matrices (GEL and SF) to inorganic phase (HAp) by XRD, SEM, and TEM. Other performances of composites, including mechanical strength, thermal stability, and cytocompatibility, were measured by universal testing machine, DTA, and *in vitro* cell culture, respectively.

2. Results and discussions

2.1. The secondary structure and crystallinity of BMSF and TSF in composites

The specimens for test were obtained by immersing air-dried GEL-TSF/HAp composite and GEL-BMSF/HAp composite into 0.5 M acetic acid aqueous solution for 24 h. Resultant samples were then rinsed and lyophilized for final use. To avoid the structural transformation of SF, all operations were kept below 40 ℃.[31] Fig. 1 exhibits the FT-IR and XRD spectra of acid-treated GEL-BMSF/HAp and GEL-TSF/HAp composite. For acid-treated GEL-BMSF/HAp composite, bands at 1703 cm^{-1}, 1626 cm^{-1}, 1236 cm^{-1}, and 695 cm^{-1} were ascribed to the β-sheet structure, while absorbance peaks at 1654 cm^{-1}, 1560 cm^{-1}, and 1229 cm^{-1} corresponded to the α-helix and random coil structure.[32] As to acid-treated GEL-TSF/HAp composite, β-sheet structure (1700 cm^{-1}, 1630 cm^{-1}, 1514 cm^{-1}, 1238 cm^{-1}, 965 cm^{-1}, and 702 cm^{-1}) and α-helix structure (901 cm^{-1} and 620 cm^{-1}) were also detected simultaneously.[33] It could be concluded that β-sheet structure and α-helix structure coexisted in both BMSF and TSF in composites. The XRD spectrum (Fig. 1B) of acid-treated GEL-BMSF/HAp composite took on three diffraction peaks at 9.8°, 20.6°, and 24.3°, which were assigned to the β-sheet structure.[32] Acid-treated GEL-TSF/HAp

composite also showed three diffraction peaks at 17.3°, 20.4°, and 23.8°, corresponding to the β-sheet structure.[33] Comparing the width of the diffaction peaks at about 20°, it could be learned that TSF had higher crystallinity than BMSF for its narrower width of diffraction peak.

2.2. Surface morphology, elemental composition and distribution, and crystalline phase structure of GEL/HAp, GEL-BMSF/HAp, and GEL-TSF/HAp composite

Fig. 2A exhibits the XRD spectra of the three sorts of composites, and the main inorganic component was confirmed to be HAp by the Power Diffraction File (PDF Card NO. 01-086-1199). EDS analysis (the inserts in the upper part of Fig. 3) was also consistent with the conclusion by the expected Ca/P ratio approximate to 1.67. From the SEM images (Fig. 3), it could be found that, the surface of composites was a little rough but there were no obvious boundarys between the organic phase and inorganic phase. And nano-HAp particles were homogeneously dispersed in the organic matrix. EDS mapping (the images next to Fig. 3D, 3E, and 3F) also showed that Ca and P were uniformly dispersed into the organic matrix. In order to compare the aspect ratio of HAp crystallites dispersed in the three sorts of composites, the crystallite size D_{hkl} (nm) of HAp was calculated by Scherrer equation:[34]

$$D_{hkl} = k\lambda/(\beta_{hkl}\cos\theta)$$

Where k is the shape factor with a value of 0.89, β_{hkl} is the full-width at half-maximum, and θ is the peak diffraction angle for (hkl) Miller's plane.

And the crystallographic parameters of HAp crystallites were obtained utilizing

the Bragg equation and formula for interplanar crystal spacing of hexagonal crystal system:

$2d\sin\theta = n\lambda \qquad 1/d^2 = 4(h^2+k^2+l^2)/3a^2+l^2/c^2$

Where θ is the peak diffraction angle for (hkl) Miller's plane, d is the interplanar crystal spacing, a and c are lattice parameters.

Unexpectedly, only (002) diffraction peak was explicitly observed in the XRD spectra while (300) diffraction peak was not strong enough to be noticed. This was because that the intense (211) diffraction peak shielded (300) diffraction peak. Thus, peak fit method was applied to separate the overlapping (211) and (300) diffraction peak. The separated diffraction peaks were exhibited in Fig. 2B-2D. Table.1 lists the calculated crystallite sizes and crystallographic parameters of HAp in the three composites. It could be learned that the aspect ratio of HAp crystallites dispersed in the three composites decreased in this order: GEL-TSF/HAp > GEL-BMSF/HAp > GEL/HAp. TEM images (Fig. 4) also confirmed the judgement.

To date, few corresponding literatures have been found reporting and explaining this phenomenon. Hereon, speculative models of the way in which self-assembly of HAp crystallites might work in the three composites (Fig. 8) were put forward in this paper. And the reason why rod-like HAp crystallites dispersed in GEL-TSF/HAp composite presented higher aspect ratio than those in GEL-BMSF/HAp and GEL/HAp composite would be detailedly discussed at the end of this section as well.

2.3. Thermal stability

TGA/DTG and DTA (Fig. 5) were carried out on the three sotrs of composites. From the TGA curves, it could be found that all samples presented two weight loss stages at 55-65 ℃ (physioabsorbed water) and 320-340 ℃ (decomposition of organic matrices). The 1st and 2nd weight loss were annotated in the TGA curves and no big differences were observed among the three composites. By simple calculation, it was found that the actual polymer/HAp ratios of GEL/HAp, GEL-BMSF/HAp, and GEL-TSF/HAp composite were 1, 0.94, and 0.92, respectively. But the starting reactant ratios (weight ratios of organic matrices to inorganic HAp) of the three composites were all maintained at 1.5. This phenomenon might be caused by the loss of organic components in the preparation process of composites. The percentage of inorganic HAp in the three composites decreased in this order: GEL-TSF/HAp (52.0%) > GEL-BMSF/HAp (51.7%) > GEL/HAp (50%). From the DTG curves, it was also discovered that the decomposition temperatures of organic components of GEL/HAp, GEL-BMSF/HAp, and GEL-TSF/HAp composite were located at 328.2 ℃, 328.8 ℃, and 333.3 ℃, respectively. In general, GEL-TSF/HAp composite was slightly thermal stable than the other two composites.

In DTA curves, GEL/HAp composite showed two endothermic peaks at 60.9 ℃ (moisture) and 395.5 ℃ (decomposition of GEL molecules).[8] For GEL-BMSF/HAp and GEL-TSF/HAp composite, endothermic peaks at about 217 ℃ corresponded to the crystallization of random-coil fibers to β-sheet nanocrystals.[26, 31] Endothermic peaks at 311 ℃ (Fig. 5B) and 329.8 ℃ (Fig. 5C) were consistent with the decomposition of BMSF and TSF, respectively.[33, 35] And the decomposition

temperatures of GEL molecules in GEL-BMSF/HAp and GEL-TSF/HAp composite were located at 510.9 ℃ (Fig. 5B) and 515.5 ℃ (Fig. 5C), respectively.[8] Comparing the decomposition temperatures of GEL molecules in the three composites, it could be concluded that GEL-TSF/HAp and GEL-BMSF/HAp were much more thermal stable than GEL/HAp while GEL-TSF/HAp was slightly more stable than GEL-BMSF/HAp.

It was deduced that this phenomenon might be accorded with the particle size of HAp crystallites. From foregoing conclusion, it was realized that rod-like HAp crystallites in GEL-BMSF/HAp and GEL-TSF/HAp composite presented higher aspect ratio than those in GEL/HAp. Generally, grain boundaries of rod-like HAp crystallites increased with the increase of aspect ratio. More grain boundaries corresponded to higher surface energy. HAp crystallites with high surface activity could intensively interact with organic phase, enhancing the thermal stability of composites.

2.4. Mechanical property

The mechanical properties of the three sorts of composites were tested in their dry states by a universal testing machine. All the samples were shaped into cylinders with height doubling diameter to meet the standards set by ASTM C39 for compression test.[36] The stress-strain curves of the three sorts of composites (Fig. 6) all showed three regions, namely a linear elasticity area, a plastic collapse-plateau, and a densification area, which were very similar to those of cancellous bone.[37] The only

difference was that there existed an obvious yield point in the stress-strain curve of GEL-TSF/HAp at strain of 0.02 (Fig. 6B). This phenomenon was thought to be related to the internal molecular structures of composites and would be illuminated in the subsequent text. The small strain, linear-elastic response of the composites resulted from the elastic bending of the cell walls of the cross-linked network. The linear-elastic region ended when the units began to collapse. Progressive compressive collapse yielded the long, horizontal plateau of the stress-strain curve, which would proceed until opposite cell walls met and touched, causing a steep increase in stress.[7] The elastic modulus was calculated via the equation below and presented in Fig. 6C.

$$E=\tan\alpha=\Delta\sigma/\Delta\varepsilon$$

Where E (elastic modulus) refers to the slope of the initial region of stress-strain curves, α is the corresponding angle of slope, σ and ε are the stress and strain, respectively. The insert in Fig. 6A exhibited the initial part of the stress-strain curves with a strain < 2%.

The calculated results showed that the elastic modulus was 1785 MPa for GEL-TSF/HAp, 1374 MPa for GEL-BMSF/HAp, and 1049 MPa for GEL/HAp. In addition, it was also found that GEL-TSF/HAp composite also showed higher compressive modulus at high strain than the other two composites. Explanations for this phenomenon lay in three aspects: the crystalline structures of organic phase, the actual HAp content in composites, and the interaction between organic phase and inorganic phase. In fact, the first one was a speculative explanation,

which was lately proposed by our research group, and not confirmed by literatures. It was assumed that the subtle deviations in secondary structures of TSF and BMSF led to the significant differences in mechanical strength of composites.[38] And it would be detailedly discussed at the end of this section as a possible model.

From aforementioned TGA data, it was found that the actual HAp contents of GEL/HAp, GEL-BMSF/HAp, and GEL-TSF/HAp composite were 50%, 51.7%, and 52%, respectively. HAp could function as an inorganic reinforcement phase and might have great influence on mechanical strength of composites.[39] It was believed that the higher actual HAp content of GEL-TSF/HAp composite contributed to its higher elastic modulus and compressive modulus to some extent. In addition, the more intense interaction between the organic phase and inorganic phase in GEL-TSF/HAp composite also made for its excellent mechanical strength. From previous DTA data, it was found that the GEL molecules in GEL-TSF/HAp had higher thermal stability than in GEL-BMSF/HAp and GEL/HAp composite. It was inferred that GEL molecules were heavily combined with HAp crystallites and there might existed strong interactions between GEL molecules and HAp crystallites (*e.g.,* electrostatic interaction, hydrogen bonds) in GEL-TSF/HAp composite.[8]

2.5. Cell affinity

For an ideal biodegradable BTE scaffold, cell affinity is an essential factor to be concerned about.[40] Materials designed for tissue engineering applications should be capable to stimulate specific cell response at molecular level and elicit specific

interactions with cell, and thereby direct cell attachment, proliferation, differentiation, and extracellular matrix production as well as organization.[41] Cell affinity commonly includes two aspects: cell attachment and cell growth. The interaction of cells with materials results from specific recognition among cell surface adhesion receptors (integrins) and extracellular matrix proteins (fibronectin, vitronectin, and collagen), which have a cell-binding domain containing the Arg-Gly-Asp (RGD) sequence.[42, 43] Very small concentrations of active peptides can have dramatic biological effects. A surface density of only 1 fmol/cm^2 of an RGD peptide effectively promotes cell adhesion to an otherwise nonadherent surface.[44] In addition; surface energy and surface roughness are also of great significance in mediating the cell adhesion.[45, 46]

Fig. 7A-7C demonstrates that MG63 cells are tightly attached to the surface of the three composites. Comparing the optical density on day 7 (Fig. 7D), more cells proliferated on GEL/HAp membrane than on GEL-BMSF/HAp and GEL-TSF/HAp membrane. Presumably, the remaining toxic reagents in BMSF and TSF (*e.g.,* LiBr, LiSCN) influenced the cytocompatibility of GEL-BMSF/HAp and GEL-TSF/HAp composite. It was also discovered that cells on GEL-TSF/HAp showed better proliferative potential than those on GEL-BMSF/HAp after 7 days.

According to the viewpoint of Das, rough surface morphology, high surface energy, and low values of contact angles were important factors for better cell materials interaction.[46] Fig. 3 exhibits the surface morphology of the three composites and it could be found that GEL-TSF/HAp composite had a rougher surface than

GEL-BMSF/HAp and GEL/HAp composite. As is mentioned before, rod-like HAp crystallites in GEL-TSF/HAp presented higher aspect ratio than those in GEL-BMSF/HAp and GEL/HAp. Accordingly, HAp crystallites in GEL-TSF/HAp had higher surface energy and lower contact angles, which could facilitate the adhesion of cells to the surface of materials. Most importantly, TSF contains more RGD peptides, which could significantly promote cell adhesion to the surface of materials. For these reasons, cells on GEL-TSF/HAp membrane showed better proliferative potential than those on GEL-BMSF/HAp membrane.

2.6. Speculative models of the way in which self-assembly of HAp crystallites might work and possible explanations for the differences in aspect ratio of HAp crystallites dispersed in the three composites

Generally, biomineralization refers to the controlled growth of bioceramics from aqueous solution, and proper organic matrices could act as the host for the nucleation and growth process.[47] For composites in this research, polar functional groups of organic matrices could function as especial active sites for the coordination of Ca^{2+} to form ion complexes. Owing to electrostatic interaction, these complexes could further interact with PO_4^{3-} and developed critical nucleis for the nucleation and growth of HAp crystallites.

For a living bone, the HAp crystals were mainly located in the small spaces within the collagen fibril (40 nm in length).[48-50] And GEL mainly consisted of denatured collagen and about 10% of GEL is re-natured collagen fibers.[51, 52] Thus, as

to GEL/HAp composite, we herein assumed that the active sites for nucleation and growth of HAp crystallites were mainly located in the hole zone (the gap between GEL molecules). Progressive growth of HAp crystallites along GEL fibril would be restricted by the spatial structure of hole zone as well as the compartments of 3D cross-linked network.[8, 53] Fig. 8A exhibits the speculative schematic diagram. However, for GEL-BMSF/HAp and GEL-TSF/HAp composite, HAp crystallites could form at not only the aforementioned hole zone but also somewhere else. Containing aspartic acid and lysine, SF could take part in the cross-linking process by schiff base reaction.[54] Therefore, some short GEL fibers might be connected by SF threads. Simultaneously, a new hole zone formed between the connected GEL fibers. Ca^{2+} and PO_4^{3-} might nucleate here, arrange, and self-assemble into HAp crystallites along the SF axis.[21] Fig. 8B shows this process.

In order to distinguish the two hole zones, the former one was defined as hole zone $1^{\#}$ and the latter one as hole zone $2^{\#}$. For reason that the gap distance of hole zone $2^{\#}$ was larger than that of hole zone $1^{\#}$, the HAp crystal nucleus in GEL-SF hydrogels was able to grow into longer HAp crystallites along the SF axis.

2.7. Speculative reinforcement model and reinforcement mechanism of TSF to GEL-TSF/HAp composite

For the hierarchical structures of silk fibers, the secondary structure could be divided into crystalline domains (the β-sheet nanocrystals) and noncrystalline (semi-amorphous) domains containing less orderly random coils and α-helices.[55]

β-sheet nanocrystals were bonded by means of assemblies of hydrogen bonds and embedded in the semi-amorphous domains.[56] From the theory of Jin and Kaplan, β-sheet nanocrystals in SF comprised of hydrophobic blocks and were surrounded by hydrophilic blocks. Thus, they took on a special spheroidal structure.[57] And these spheroidal crystals of SF would have great influence on its mechanical strength.[58]

In this research, SF fibers took part in the crosslinking process by schiff base reaction. The upper part of Fig. 9 showed the schematic diagram. When the composites were compressed, the compartments of cross-linked network began to deform.[7] For GEL-BMSF/HAp and GEL-TSF/HAp, it was deduced that the compressed compartments would be impeded by the semi-amorphous domains of SF along the direction of slipping. The lower part of Fig. 9 explicitly exhibited this process. This process mainly corresponded to the linear-elastic region and would continue until the semi-amorphous domains were heavily compacted. Once the semi-amorphous domains being densified, a yielding process took place, which could be seen in the stress-strain curve of GEL-TSF/HAp in Fig. 6B. This explained that calculated elastic modulus values of GEL-BMSF/HAp and GEL-TSF/HAp were higher than that of GEL/HAp to some extent.

Containing a larger number of polar functional groups, the semi-amorphous domains of TSF were subjected to stronger space charge repulsion effect, and therefore became stiffer and resilient just like a helical spring.[18, 21] This was why GEL-TSF/HAp composite showed higher elastic modulus than GEL-BMSF/HAp composite at low strain.

Presumably, the higher compressive modulus at high strain of GEL-TSF/HAp than that of GEL-BMSF/HAp and GEL/HAp was related to the special amino acid sequence and high crystallinity of β-sheet nano-crystals in TSF. At the end of linear-elastic region, the rigid β-sheet nano-crystals began to sustain the external stress imposed by the deformed compartments owing to the densification of semi-amorphous domains (shown in Fig. 9B). Maybe the fact that the key interaction in β-sheet nanocrystals are hydrogen bonds, one of the weakest chemical bonds known, made us doubt that whether the β-sheet nanocrystals were stiff enough to bear the high load. Keten made it clear. Engineering materials generally depend on strong bonding, which needs considerable energy use during synthesis that could also render catastrophic failure once bonds break. In contrast, the use of weak hydrogen bonding facilitates self-assembly at moderate temperature and the broken hydrogen bonds are capable to reform because of its built-in capacity to self-heal.[27]

As it has been noted, antiparallel β-sheet crystals at nanoscale, consist of highly conserved poly—$(Gly\text{-}X)_n$—(X represents Ala or Trp residues) and poly—$(Ala)_n$— sequence for BMSF and TSF, respectively. Fig. 6D exhibits the special molecular structures of the β-sheet nanocrystals in BMSF and TSF. Obviously, the β-sheet nanocrystals in BMSF were subjected to stronger steric-hindrance effect and had less compact molecular structure than TSF because of the huge side groups. Consequently, it was more prone for β-sheet nano-crystals in TSF to transfer the load between chains under lateral loading

instead of collapsing.

Besides, according to the theory of Keten, nanoscale confinement of β-sheet nanocrystals greatly influenced the stiffness, resilience, and fracture toughness of SF at molecular level.[27] Smaller nano-crystals are stronger and tougher. This is owing to that large β-sheet nanocrystals are soft and failed catastrophically at low force because of formation of the crack-like flaw. And this flaw will in turn accelerate the disintegration because of the easier access of competing water molecules to hydrogen bonds that facilitate rupture.[59] It was clear that the size of β-sheet nanocrystals in BMSF was larger than those in TSF for the existence of huge side groups.

From previous characterizations, it was also found that TSF in GEL-TSF/HAp composite had higher crystallity than BMSF in GEL-BMSF/HAp composite. Thus, there were more β-sheet nanocrystals in GEL-TSF/HAp than in GEL-BMSF/HAp hindering the slipping of organic network.

3. Experimental section

3.1. Materials

The *Bombyx mori* silkworm cocoons and tussah silkworm cocoons were bought from Nanyang, Henan, China. Gelatin with gel strength ~240 g bloom and lithium bromide (LiBr) were purchased from Aladdin Industrial Co.,Ltd. (Shanghai, China). Calcium nitrate tetrahydrate ($Ca(NO_3)_2{\cdot}4H_2O$), diammonium hydrogen phosphate ($(NH_4)_2HPO_4$), acetic acid, glutaraldehyde, ammonia, ammonium thiocyanate

(NH_4SCN), and lithium hydroxide monohydrate ($LiOH·H_2O$) were obtained from Sinopharm Chemical Reagent Co.,Ltd. (Shanghai, China) and were all of analytical grade. All chemicals were used without any further purification. Deionized ultrapure water was used throughout the experiment. For cytotoxicity assay, the MG63 osteoblast-like cells were generously supplied by Wuhan University School of Stomatology (Wuhan, China).

3.2. Preparation of regenerated BMSF solution

Bombyx mori silkworm cocoons were degummed in 0.5% (w/v) Na_2CO_3 aqueous solution at 100 ℃ for 30 min and then washed thoroughly with deionized water to remove the silk sericin. The degumming silk fibroin fibers were dissolved in 9.3 M LiBr solution (liquor ratio=15:1) at 40 ℃ and as-prepared solution was then dialyzed against deionized ultrapure water for 3 days.[32] As a result, regenerated BMSF solution was obtained and the final solid content of the solution was 2.34%, which was calculated by weighing method.

3.3. Preparation of regenerated TSF solution

3.3.1. Preparation of LiSCN aqueous solution

Firstly, 67.184 g $LiOH \cdot H_2O$, 121.792 g NH_4SCN were added into 400 mL deionized water with agitation at 70 ℃ for 2 h. Under this condition, a chemical reaction took place and the entire process could be described by the following equation:

$$LiOH \cdot H_2O + NH_4SCN = LiSCN + NH_3 \cdot H_2O + H_2O$$

Then, the resultant solution was transferred into a rotary evaporator and distilled

under reduced pressure at 80 ℃ to remove the generated NH_3 and H_2O. Next, a certain volume of deionized H_2O was poured into the remaining solution to make the final volume of 100 mL. Consequently, 16 M LiSCN aqueous solutions were prepared.

3.3.2. Dissolution of TSF and post-treatment

First, tussah silkworm cocoons were degummed as the same way we did with *Bombyx mori* silkworm cocoons. Then, the degumming tussah fibers were dissolved in 16 M LiSCN aqueous solution with a liquor ratio of 15:1 at 40 ℃. In the whole dissolution process, 0.1 g tussah fiber was added every time to guarantee the complete dissolution of TSF. Afterwards, the turbid solution was filtered by gauze first and then by filter paper to remove the undissolved part. The filtrate was dialyzed against deionized water for 3 days. The remaining solution was ulteriorly filtered by 0.8 μm millipore filter for twice under reduced pressure. The solid content of regenerated TSF solution was 0.87%.

3.4. Preparation of GEL-TSF/HAp and GEL-BMSF/HAp nano-composites

The organic/inorganic ratio of the two composites was kept at 60/40 while the GEL/SF ratio was kept at 5/1. The preparation process was detailedly depicted in the subsequent text. Firstly, transparent GEL solution was synthesized by dissolving 0.4 g GEL into a certain volume of acetic acid solution at 40 ℃ for 1 h. Then, 0.252 g $(NH_4)_2HPO_4$ and 0.752 g $Ca(NO_3)_2 \cdot 4H_2O$ (Ca/P=1.67) were successively added into the GEL solution. The stir was kept at 40 ℃ for 0.5 h for the thorough dispersion of PO_4^{3-} and Ca^{2+} into GEL solution. After that, a certain quality of TSF solution or

BMSF solution was dripped into the GEL solution slowly with gentle agitation. The final volume of the solution was maintained at 40 mL. 2 minutes later, 300 μL glutaraldehyde solutions were poured into the solution and 1 more minute's agitation was carried out. The resultant solution was then placed in a refrigerator (0 ℃) for more than 12 h. Under this operating condition, the solution gelled into solidified hydrogel. Afterwards, ammonia was poured on the surface of the hydrogel through the permeation from the top to the bottom. In this alkaline environment, *in situ* precipitation took place and the entire process could be described by the following chemical reaction: [60]

$$10Ca^{2+} + 6HPO_4^{2-} + 8OH^- = Ca_{10}(PO_4)_6(OH)_2 (\downarrow) + 6H_2O \ (pH>10)$$

After the mineralization, the ultimate composite materials were rinsed with deionized water for several times until the pH of the eluate was about 7. For comparison, the above-mentioned process has been repeated in the absence of SF to fabricate the GEL/HAp hydrogel.

3.5. In vitro cell culture

3.5.1. Cell proliferation

Cytotoxicity of composites toward MG63 osteoblast-like cells was investigated using cell counting kit-8 assay (CCK-8; Dojindo Laboratories, Japan). Briefly, the MG63 cells (2.0×10^3 cells/well) were seeded on 8 mm disc-shaped membranes of composites placed in 96 well cell culture plates (Corning Life Sciences) and incubated in Dulbecco's modified Eagle medium (DMEM) containing 10% fetal bovine serum

(FBS) and 1% antibiotis at 37 ℃ in a 5% CO_2 incubator. A sample was taken out and rinsed with Phosphate Buffer Solution (PBS) at pre-determined time points (1 d, 4 d, and 7 d). A mixture of 270 μL medium and 30 μL CCK-8 reagent was added to each sample and cultured for 2 h at 37 ℃. Then, the remaining medium was transferred into another 96 well plates for the measurement of optical density (O.D) using an ELX808 Ultra Micro plate Reader (Bio-Tek Instruments, Inc., America). Five parallel replicates were read for each sample. The results were expressed as the means of the absorbance data.

3.5.2. Cell attachment

Attachment of MG63 cells to the three sorts of composite membranes was observed by SEM. Briefly speaking, after 4 days' cultivation, membranes with cells growing on were rinsed with PBS twice. Then these membranes were soaked in 2.5% glutaraldehyde solution at 4 ℃ for the fixing of cells. Resultant membranes were dehydrated by ethanol in an increasing concentration gradient, and then lyophilized for final observation.

3.5.3. Statistical analysis

Statistical analysis was carried out by one-way analysis of variance (ANOVA) and Tukey procedure for post hoc comparison using Graphpad Prism 5. $p<0.05$ was considered statistically significant.

3.6. Characterization

Morphological and structural investigations were carried out by an

environmental scanning electron microscope (ESEM) (Quanta200, FEI, Holland), a field emission scanning electron microscope (FE-SEM) (Sigma, Zeiss, Cermany) and a field emission transmission electron microscope (FE-TEM) (JEM-2100, JOEL, Japan). Semiquantitative elemental analysis of composites was carried out by SEM-associated energy-dispersive spectroscopy (EDS) area analysis (EDAX GENSIS, AMETEK, America). The crystal phase was investigated using wide angle X-ray diffraction analysis (XRD; X'pert PRO, Panalytical, Holland). The working condition of XRD was CuK_0 radiation (wavelength: λ=0.15406 nm) via a rotating anode at 40 kV and 40 mA. The data were collected in step of 0.1° and range of scattering angles (2θ) from 10° to 80°.

Compositional and structural determination of the TSF and BMSF in composites was characterized by Fourier Transform Infrared Spectrometer (FT-IR, Nicolet5700, America) and XRD (X'pert PRO, Panalytical, Holland).

Thermal stability of composites was investigated using thermogravimetric analysis (TGA) and differential thermal analysis (DTA) (Diamond TG/DTA, Perkin Elmer, America). Experiments have been performed using simultaneous TGA-DTA by heating samples at 20 Cel/min in a temperature range between 20 ℃ and 600 ℃ in nitrogen atmosphere .

Compression tests were performed by a universal testing machine (SHIMADZU, AGS-J, Japan). All specimens were shaped into cylinders (4 mm in height, 2 mm in diameter). Samples were compressed in a direction perpendicular to the cross section

of cylinders at a cross-head speed of 0.5 mm/min. Elastic modulus was calculated as slope of the initial linear portion of stress–strain curve (strain < 2%) and expressed as means of three replicates. Elastic modulus at low strain and compressive modulus at high strain were considered as basic principles to evaluate the mechanical strength of a material in this study.

4. Conclusions

Three sorts of composites (*i.e.,* GEL-TSF/HAp, GEL-BMSF/HAp, and GEL/HAp) were prepared by a novel *in situ* precipitation method in this study. Characterizations, including composition, morphology, structures of crystalline phase, mechanical strength, thermal stability, and cytocompatibility, showed that GEL-TSF/HAp composite could be an ideal BTE substitute. Comparisons between GEL-TSF/HAp and GEL-BMSF/HAp composite indicated that GEL-TSF/HAp had advantages over GEL-BMSF/HAp on mechanical strength and *in vitro* cytocompatibility. Moreover, it was deduced that the deviations in secondary structure and crystallinity of TSF and BMSF caused the differences in mechanical strength between GEL-TSF/HAp composite and GEL-BMSF/HAp composite.

Acknowledgements

This research was supported by the National Natural Science Foundation of China (Nos. 31071265 and 30900297) and the National Basic Research Program of China (973 Program) (2012CB725300)

References

1. A.-M. Yousefi, H. Oudadesse, R. Akbarzadeh, E. Wers and A. Lucas-Girot, *Nanotechnology*

Reviews, 2014, **3**.
2. Q. Zhang, K. Tan, Y. Zhang, Z. Ye, W.-S. Tan and M. Lang, *Biomacromolecules*, 2014, **15**, 84-94.
3. M. Swetha, K. Sahithi, A. Moorthi, N. Srinivasan, K. Ramasamy and N. Selvamurugan, *Int J Biol Macromol*, 2010, **47**, 1-4.
4. M. M. Stevens, *Materials Today*, 2008, **11**, 18-25.
5. S. J. Hollister, *Nat. Mater.*, 2005, **4**, 518-524.
6. L. J. Zhang and T. J. Webster, *Nano Today*, 2009, **4**, 66-80.
7. S. Wu, X. Liu, K. W. K. Yeung, C. Liu and X. Yang, *Materials Science and Engineering: R: Reports*, 2014, **80**, 1-36.
8. M. C. Chang, C.-C. Ko and W. H. Douglas, *Biomaterials*, 2003, **24**, 2853-2862.
9. X. Liu, L. A. Smith, J. Hu and P. X. Ma, *Biomaterials*, 2009, **30**, 2252-2258.
10. W. W. Thein-Han and R. D. K. Misra, *Acta Biomaterialia*, 2009, **5**, 1182-1197.
11. H. R. Lin and Y. J. Yeh, *Journal of biomedical materials research. Part B, Applied biomaterials*, 2004, **71**, 52-65.
12. D. Pasqui, P. Torricelli, M. De Cagna, M. Fini and R. Barbucci, *Journal of biomedical materials research. Part A*, 2014, **102**, 1568-1579.
13. R. A. A. Muzzarelli, *Carbohydrate polymers*, 2011, **83**, 1433-1445.
14. D. Puppi, F. Chiellini, A. M. Piras and E. Chiellini, *Prog. Polym. Sci.*, 2010, **35**, 403-440.
15. H. W. Kim, J. H. Song and H. E. Kim, *Advanced Functional Materials*, 2005, **15**, 1988-1994.
16. C. Krywka, I. Krasnov, R. Figuli, M. Burghammer and M. Müller, *Macromolecules*, 2014, **47**, 7187-7193.
17. G. H. Altman, F. Diaz, C. Jakuba, T. Calabro, R. L. Horan, J. S. Chen, H. Lu, J. Richmond and D. L. Kaplan, *Biomaterials*, 2003, **24**, 401-416.
18. L. Wang and C. Li, *Carbohydrate polymers*, 2007, **68**, 740-745.
19. Z.-L. Mou, L.-M. Duan, X.-N. Qi and Z.-Q. Zhang, *Materials Letters*, 2013, **105**, 189-191.
20. Y. Tamada, *Biomacromolecules*, 2005, **6**, 3100-3106.
21. J. X. He, D. W. Wang and S. Z. Cui, *Polymer Bulletin*, 2012, **68**, 1765-1776.
22. J. X. He, Y. Wang, S. Z. Cui, Y. Y. Gao and S. Y. Wang, *Iranian Polymer Journal*, 2010, **19**, 625-633.
23. R. Liu, J. Ming, H. Zhang and B. Zuo, *Fibers and Polymers*, 2012, **13**, 613-617.
24. H. Y. Kweon and Y. H. Park, *J. Appl. Polym. Sci.*, 1999, **73**, 2887-2894.
25. H. Kweon and Y. H. Park, *J. Appl. Polym. Sci.*, 2001, **82**, 750-758.
26. J. He, Y. Qin, S. Cui, Y. Gao and S. Wang, *Journal of Materials Science*, 2010, **46**, 2938-2946.
27. S. Keten, Z. Xu, B. Ihle and M. J. Buehler, *Nat Mater*, 2010, **9**, 359-367.
28. W. Zhang, J. X. He and S. Z. Cui, in *New Materials and Advanced Materials, Pts 1 and 2*, eds. Z. Y. Jiang, J. T. Han and X. H. Liu, 2011, vol. 152-153, pp. 734-738.
29. S. Bhumiratana, W. L. Grayson, A. Castaneda, D. N. Rockwood, E. S. Gil, D. L. Kaplan and G. Vunjak-Novakovic, *Biomaterials*, 2011, **32**, 2812-2820.
30. L. Wang, R. Nemoto and M. Senna, *Journal of the European Ceramic Society*, 2004, **24**, 2707-2715.
31. J. Magoshi, Y. Magoshi, S. Nakamura, N. Kasai and M. Kakudo, *Journal of Polymer Science: Polymer Physics Edition*, 1977, **15**, 1675-1683.

32. C. M. Li, C. Vepari, H. J. Jin, H. J. Kim and D. L. Kaplan, *Biomaterials*, 2006, **27**, 3115-3124.
33. F. Zhang, B. Q. Zuo, H. X. Zhang and L. Bai, *Polymer*, 2009, **50**, 279-285.
34. C. Li, X. Ge, G. Li, Q. Gao and R. Ding, *Advanced Powder Technology*, 2014, **25**, 1661-1666.
35. S. De-bing, D. Zhi-hui and F. Wei-guo, *J. Appl. Polym. Sci.*, 2009, **111**, 1471-1477.
36. C.-C. Ko, M. Oyen, A. M. Fallgatter, J.-H. Kim, J. Fricton and W.-S. Hu, *Journal of Materials Research*, 2011, **21**, 3090-3098.
37. J. W. Pugh, R. M. Rose and E. L. Radin, *Journal of Biomechanics*, 1973, **6**, 657-670.
38. S. P. Narayanan, A. Maeno, H. Matsuo, M. Oda, H. Morii and K. Akasaka, *Biophysical journal*, 2012, **102**, L8-L10.
39. X. Cai, H. Tong, X. Shen, W. Chen, J. Yan and J. Hu, *Acta Biomaterialia*, 2009, **5**, 2693-2703.
40. J. Yang, J. Z. Bei and S. G. Wang, *Biomaterials*, 2002, **23**, 2607-2614.
41. I. Armentano, M. Dottori, E. Fortunati, S. Mattioli and J. M. Kenny, *Polymer Degradation and Stability*, 2010, **95**, 2126-2146.
42. K. Anselme, *Biomaterials*, 2000, **21**, 667-681.
43. J. Dobkowski, R. Kolos, J. Kaminski and H. M. Kowalczynska, *Journal of biomedical materials research*, 1999, **47**, 234-242.
44. D. A. Barrera, E. Zylstra, P. T. Lansbury and R. Langer, *Journal of the American Chemical Society*, 1993, **115**, 11010-11011.
45. S. Bose, S. Dasgupta, S. Tarafder and A. Bandyopadhyay, *Acta Biomaterialia*, 2010, **6**, 3782-3790.
46. K. Das, S. Bose and A. Bandyopadhyay, *Acta Biomaterialia*, 2007, **3**, 573-585.
47. G. K. Toworfe, R. J. Composto, I. M. Shapiro and P. Ducheyne, *Biomaterials*, 2006, **27**, 631-642.
48. J.-Y. Rho, L. Kuhn-Spearing and P. Zioupos, *Medical engineering & physics*, 1998, **20**, 92-102.
49. S. Weiner and W. Traub, *The FASEB journal*, 1992, **6**, 879-885.
50. W. Landis, *Bone*, 1995, **16**, 533-544.
51. C. I. Branden, *Introduction to protein structure*, Garland Science, 1999.
52. A. Veis, *the macromolecular chemistry of gelatin,* 1964.
53. X. Shen, H. Tong, T. Jiang, Z. Zhu, P. Wan and J. Hu, *Composites Science and Technology*, 2007, **67**, 2238-2245.
54. M. C. Chang, C. C. Ko and W. H. Douglas, *Biomaterials*, 2003, **24**, 3087-3094.
55. J. D. van Beek, S. Hess, F. Vollrath and B. H. Meier, *Proceedings of the National Academy of Sciences of the United States of America*, 2002, **99**, 10266-10271.
56. S. Keten and M. J. Buehler, *Phys. Rev. Lett.*, 2008, **100**, 4.
57. H.-J. Jin and D. L. Kaplan, *Nature*, 2003, **424**, 1057-1061.
58. I. M. Ward and D. W. Hadley, *An introduction to the mechanical properties of solid polymers*, John Wiley & Sons Ltd.; John Wiley & Sons, Inc., 1993.
59. M. Sotomayor and K. Schulten, *Science*, 2007, **316**, 1144-1148.
60. L. Chen, J. Hu, J. Ran, X. Shen and H. Tong, *Int J Biol Macromol*, 2014, **65**, 1-7.

Samples	β_{002}(°)	$2\theta_{002}$(°)	D_{002}(nm)	β_{300}(°)	$2\theta_{300}$(°)	D_{300}(nm)	a(nm)	c(nm)	D_{002}/D_{300}
GEL/HAp	0.358	25.915	22.53	0.9971	32.70	8.21	0.9481	0.6284	4.14
GEL-BMSF/HAp	0.306	25.912	26.35	0.9864	32.75	8.30	0.9464	0.6300	4.77
GEL-TSF/HAp	0.299	25.901	26.97	0.9824	32.77	8.33	0.9471	0.6311	4.84

Table. 1 Crystal sizes and crystallographic parameters of HAp crystallites in the three composites

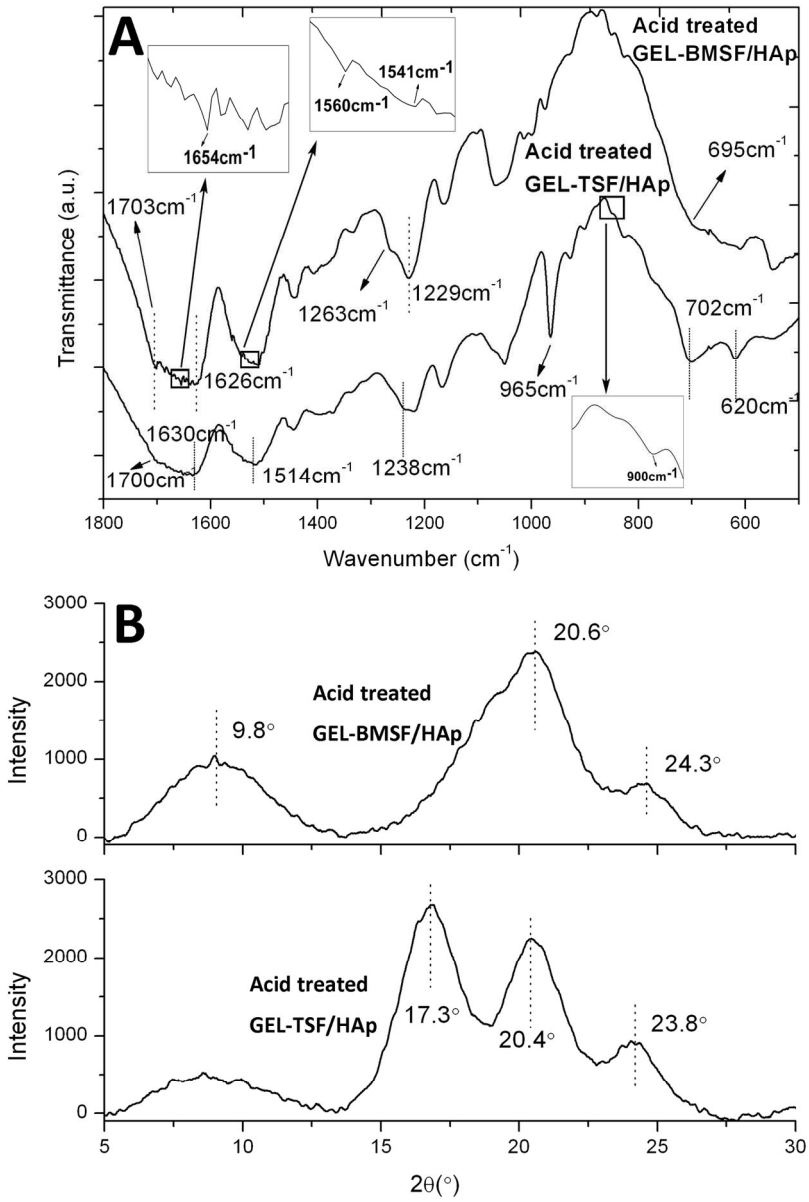

Fig. 1 (A) FT-IR spectra and (B) XRD spectra of the remaining parts of acid-treated GEL-TSF/HAp composite and GEL-TSF/HAp composite
63x93mm (600 x 600 DPI)

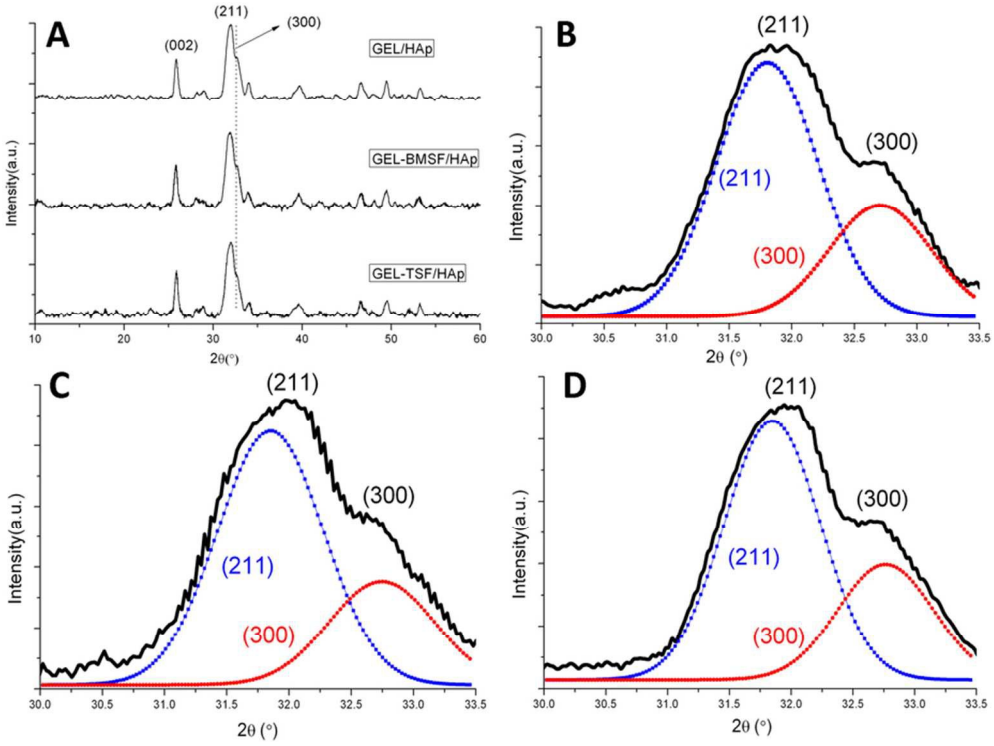

Fig. 2 (A) XRD spectra of GEL/HAp, GEL-BMSF/HAp, and GEL-TSF/HAp composite; separated (211) and (300) diffraction peaks of HAp dispersed in (B) GEL/HAp, (C) GEL-BMSF/HAp, and GEL-TSF/HAp.
39x29mm (600 x 600 DPI)

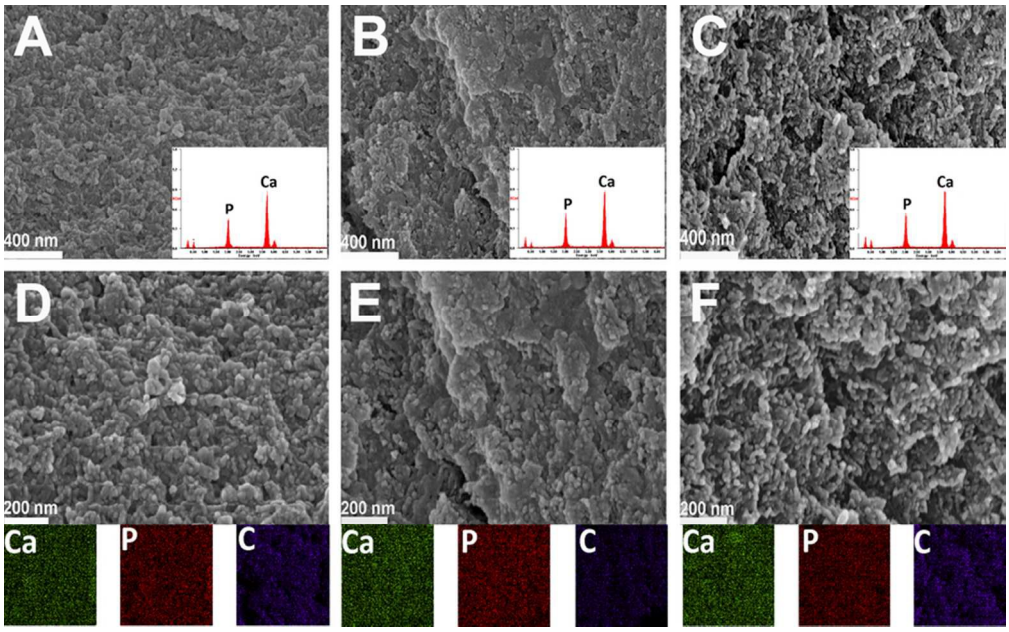

Fig. 3 Low-magnified (the upper part) and high-magnified (the lower part) SEM images of (A, D) GEL/HAp, (B, E) GEL-BMSF/HAp, and (C, F) GEL-TSF/HAp; the inserts in (A), (B), and (C) show the EDS analysis of GEL/HAp, GEL-BMSF/HAp, and GEL-TSF/HAp, respectively; the images next to (D), (E), and (F) show the corresponding EDS mapping of GEL/HAp, GEL-BMSF/HAp, and GEL-TSF/HAp, respectively.
39x24mm (600 x 600 DPI)

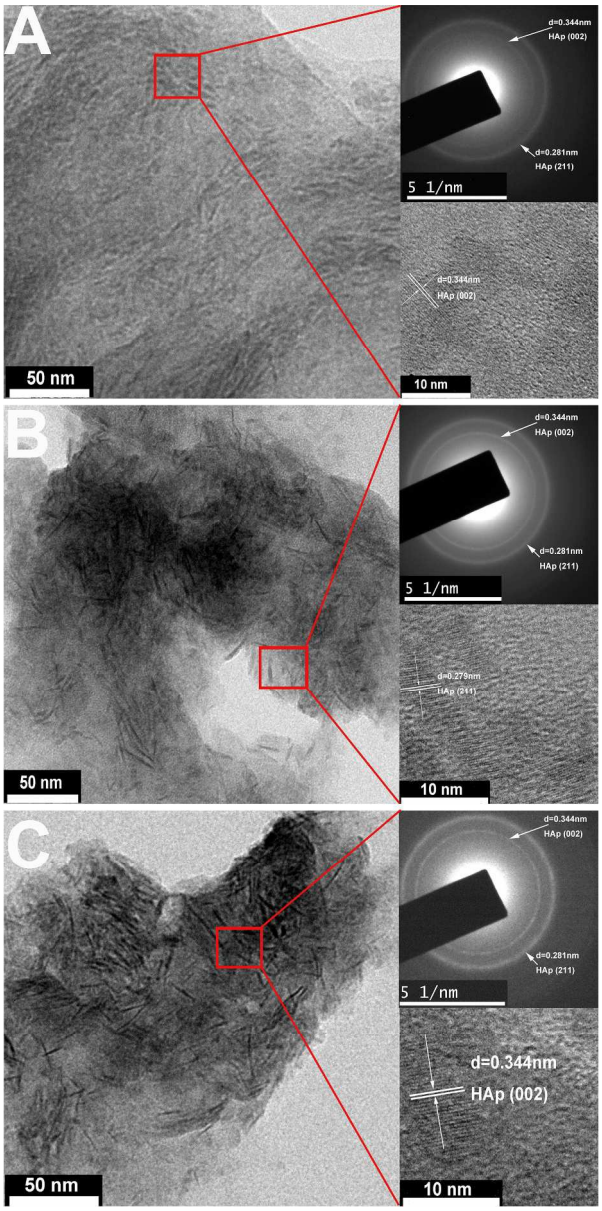

Fig. 4 TEM images of (A) GEL/HAp, (B) GEL-BMSF/HAp, and (C) GEL-TSF/HAp; the right part next to each image shows corresponding selected area electron diffraction images and high-magnified images of the marked area in the left part.
256x516mm (300 x 300 DPI)

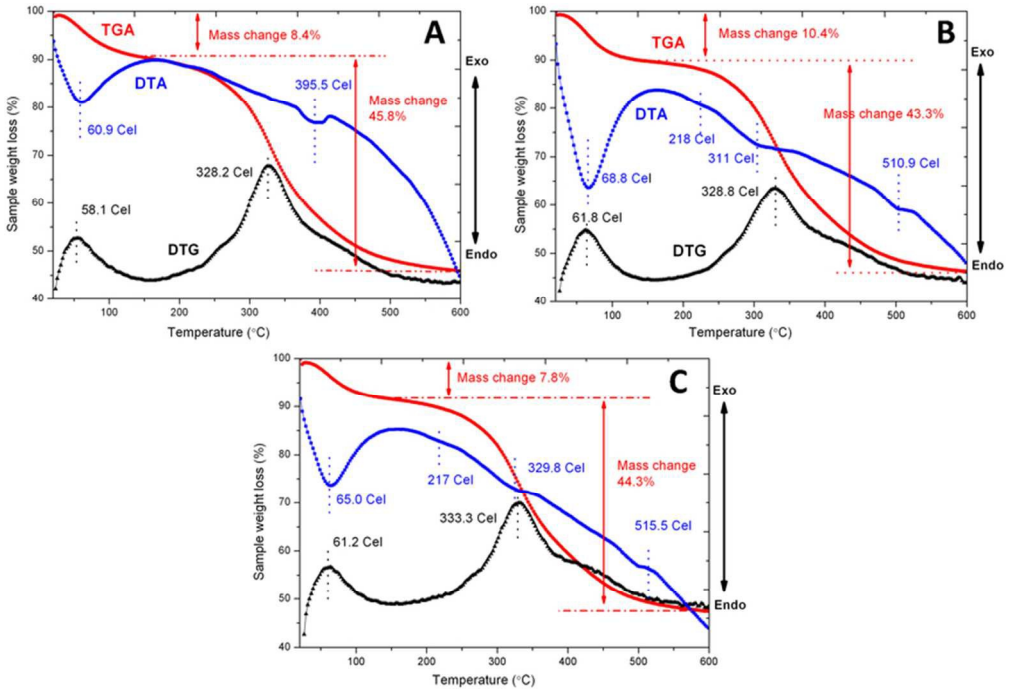

Fig. 5 TGA, DTG, DTA curves of (A) GEL/HAp, (B) GEL-BMSF/HAp, and (c) GEL-TSF/HAp.
36x24mm (600 x 600 DPI)

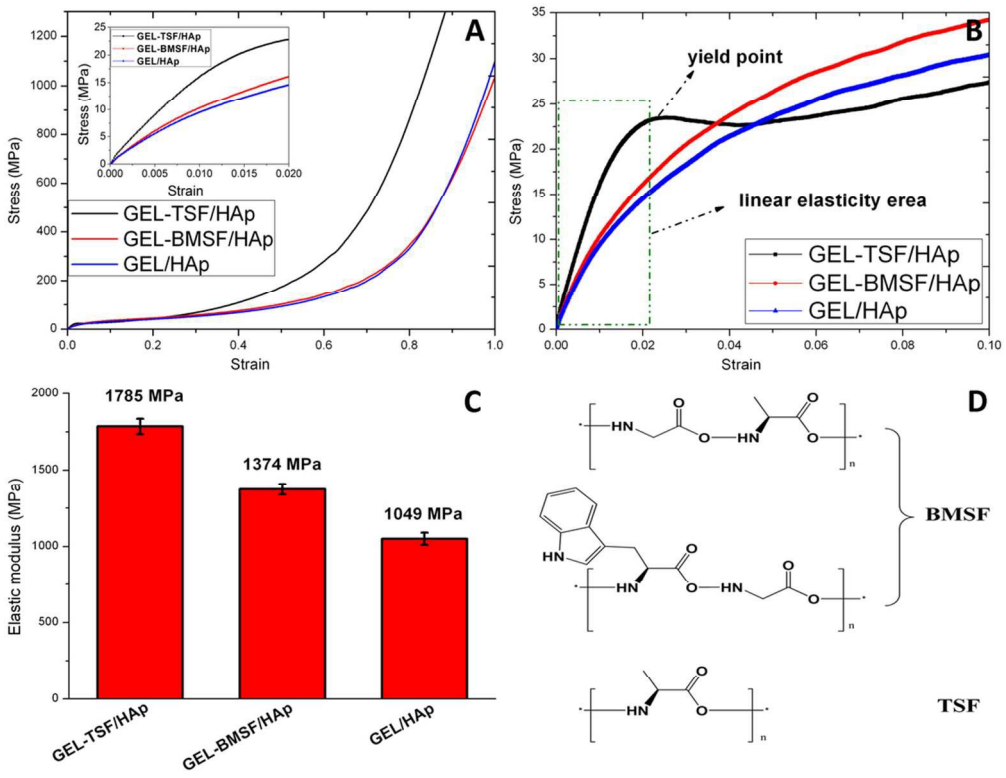

Fig. 6 (A) typical stress-strain curves of the three composites (the insert show the initial part with strain <2%); (B) stress-strain curves of the three composites with strain ranging from 0 to 10%; (C) column chart of calculated elastic modulus of the three composites; (D) molecular structure of β-sheet crystallites in BMSF and TSF
48x37mm (600 x 600 DPI)

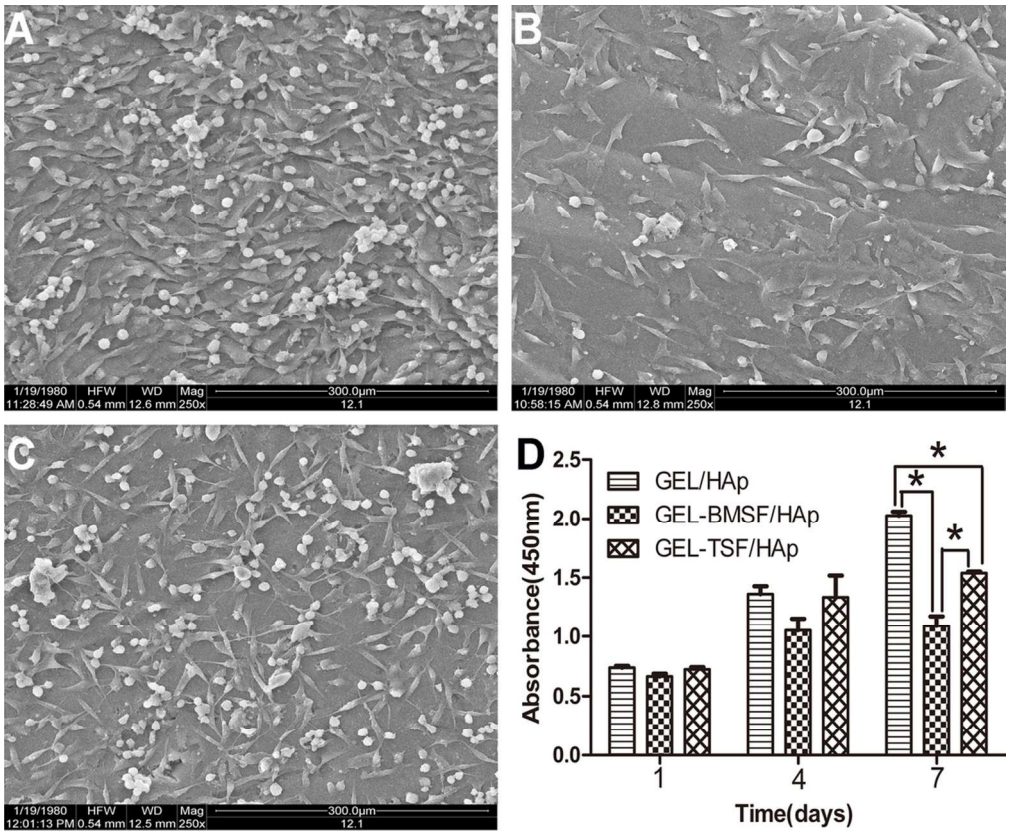

Fig. 7 Morphology of MG63 cells seeded on membranes of (A) GEL/HAp, (B) GEL-BMSF/HAp, and (C) GEL-TSF/HAp; (D) CCK-8 assay of MG63 cells on the three composite membranes. * indicates statistical significance at $p < 0.05$ by one way ANOVA with Turkey test.
52x43mm (600 x 600 DPI)

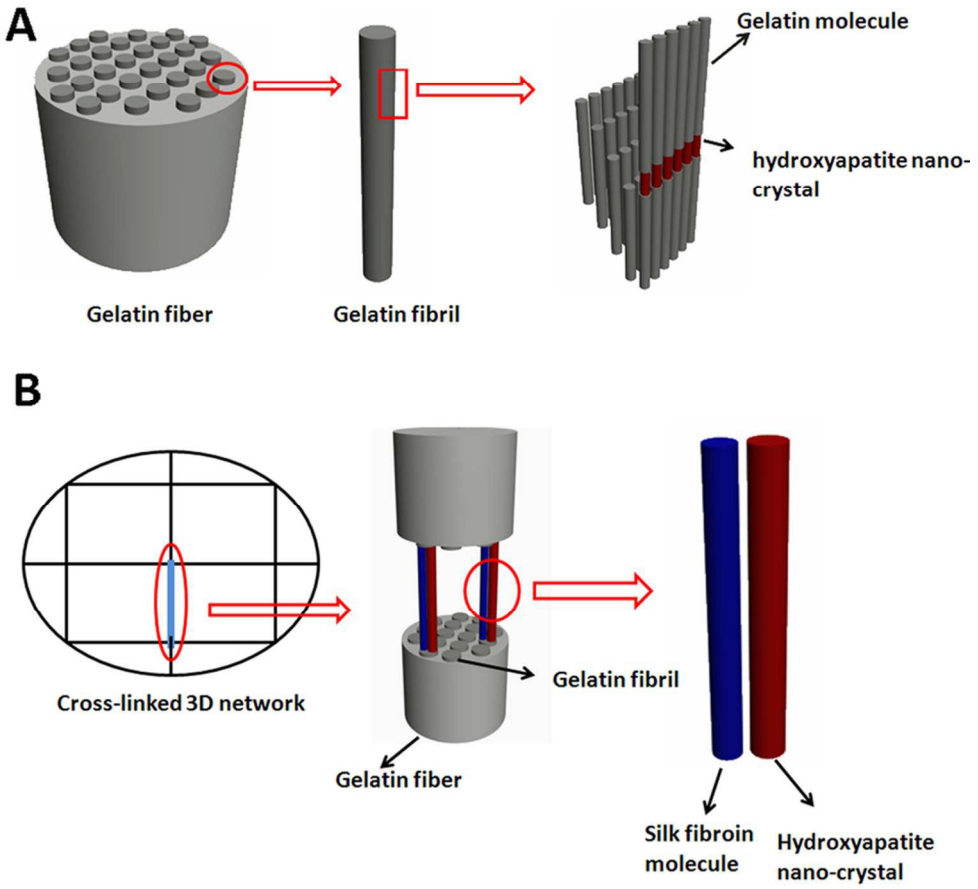

Fig. 8 Speculative schematic diagrams of nucleation and growth of HAp crystallites in (A) GEL/HAp and (B) GEL-SF/HAp composite.
40x38mm (600 x 600 DPI)

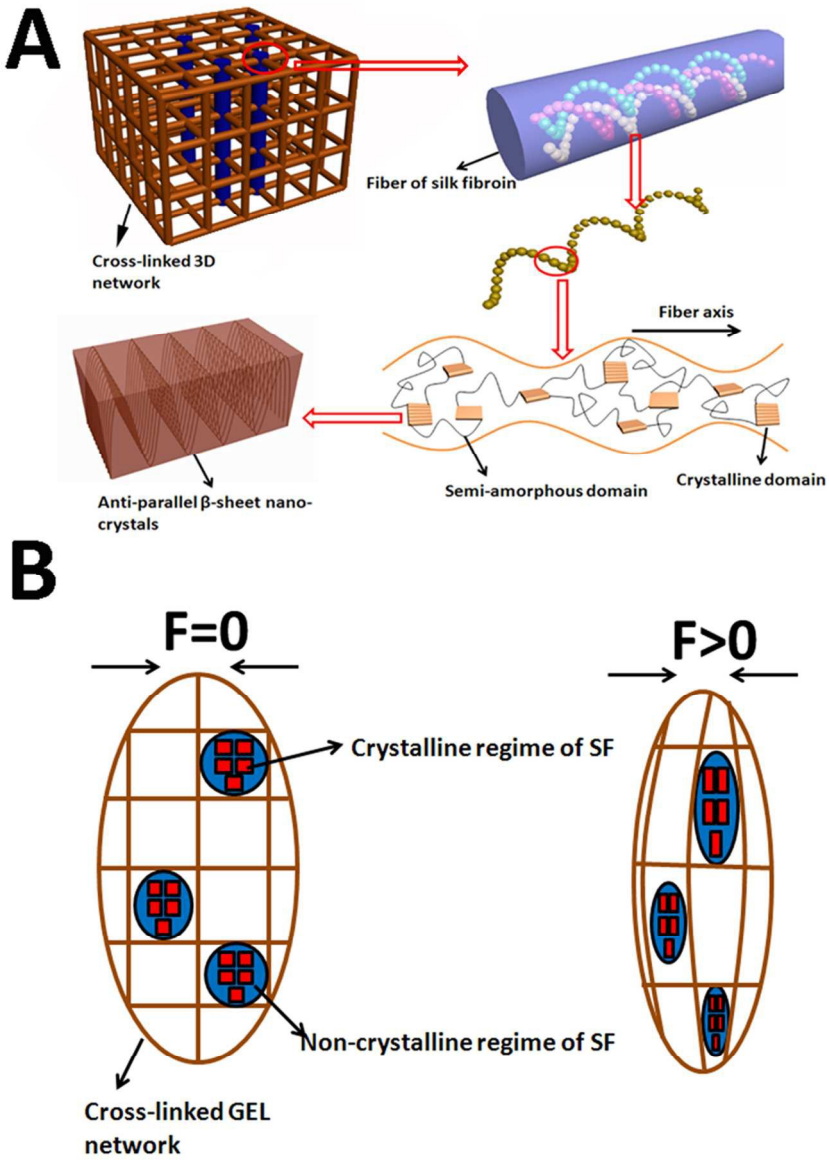

Fig. 9 (A) schematic diagram of the hierarchical structures of SF; (B) speculative schematic diagram of the impeding effect of β-sheet nano-crystals in SF to the 3D GEL network.
58x80mm (600 x 600 DPI)

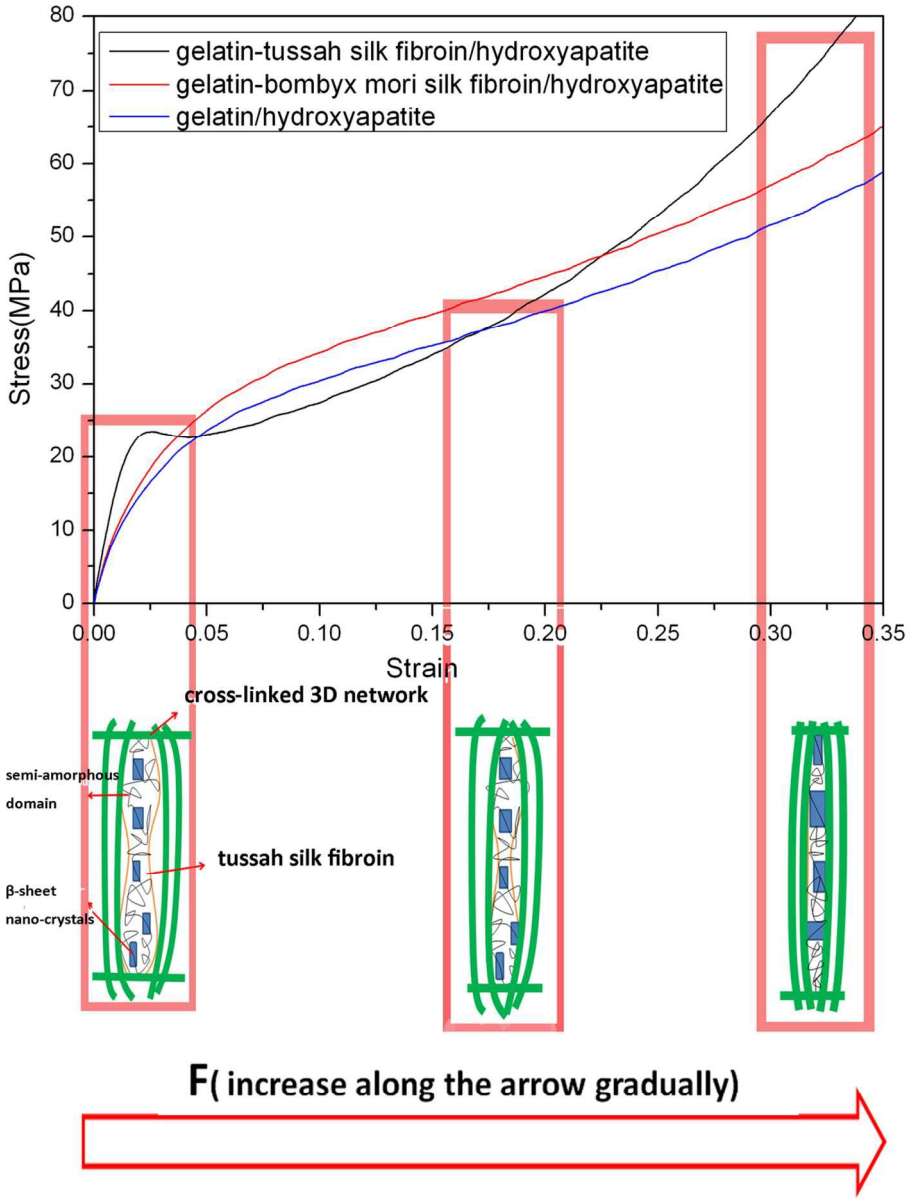

enhancement mechanism of tussah silk fibroin to gelatin-tussah silk fibroin/hydroxyapatite composite
52x69mm (600 x 600 DPI)